International Journal of Engineering Sciences and Technologies

Int. J. Eng. Sci. Technol.
2024.2(2).2
ISSN：2960-0960
https://doi.org/10.58531/ijest/2/2/2

Article

Study on the Stability of Stratified Shale Boreholes under Multi-Field Coupling

Zengbao Zhang

Western Oil and Gas Exploration Project Department, Shengli Oilfield Branch Company Dongying, 257000

Abstract: This paper investigates the stability of stratified shale boreholes in the Longmaxi Formation of the Silurian system in the Sichuan Basin, with shale gas reservoirs ranging in thickness from 65m to 516m. Considering that borehole stability is a crucial factor in drilling operations, this study combines theoretical analysis and laboratory experiments to explore the anisotropic strength characteristics of stratified shale and its borehole instability mechanisms. The research indicates that geo-stress, temperature, chemical interactions, and seepage effects significantly impact borehole stability. When considering only stress effects, the critical lower limit of drilling fluid density to prevent borehole collapse ranges from 1.3 to 1.7 g/mL. Particularly in horizontal wells with azimuth angles of 0°-40° and 180°-360°, the critical lower limit of drilling fluid density is the highest, reaching over 1.65 g/mL. However, under multi-field coupling effects, the distribution range of critical drilling fluid density increases to 1.75^{-2} g/mL, and the stability of the borehole shows significant changes in the required drilling fluid density. In horizontal wells with azimuth angles of 0°-40° and 180°-360°, the critical lower limit of drilling fluid density is the highest, exceeding 2 g/mL. In contrast, in boreholes with an azimuth angle of 120° and an inclination angle of 60°, the critical lower limit of drilling fluid density is the lowest, indicating better borehole stability in this region. The study of drilling fluid density distribution under different working conditions reveals that borehole trajectory significantly affects borehole stability. Adjustments in drilling fluid density are necessary to ensure borehole stability under specific combinations of azimuth and inclination angles. The results suggest that in actual drilling operations, it is essential to comprehensively consider factors such as stress, temperature, chemical interactions, and seepage to optimize drilling fluid density, thereby enhancing borehole stability and drilling efficiency. In conclusion, this paper establishes a multi-field coupled borehole stability model, elucidates the stability patterns of anisotropic

Citation: Zhang Z. Study on the Stability of Stratified Shale Boreholes under Multi-Field Coupling. *Int. J. Eng. Sci. Technol.*, 2024, 2(2), doi: 10.58531/ijest/2/2/2

shale under complex borehole trajectories and multi-field coupling effects, and proposes corresponding optimization recommendations for drilling fluid density. This provides theoretical foundations and technical support for the safe and efficient development of shale gas reservoirs.

Keywords: Layered shale; Wellbore stability; Multiple coupling; Anisotropic; Collapse pressure

1. Introduction

Shale gas is an unconventional resource, and the Longmaxi Formation of the Silurian system in the Sichuan Basin, with shale thickness ranging from 65m to 516m, is an ideal prospect for exploration and development [1-3]. However, previous drilling experiences and related studies have identified frequent complications in this region, such as blockages, sticking, and collapse, resulting in significant economic losses. Instability of shale formations during drilling operations is thus a critical concern [4-8]. Therefore, it is necessary to explore the anisotropic strength and borehole instability mechanisms based on laboratory experiments and theoretical analyses.

Extensive research has been conducted globally on borehole stability in drilling operations, focusing primarily on near-wellbore stress distribution and surrounding rock strength criteria. To assess the stress concentration around the borehole after drilling, Westergaard [0] initially proposed an elasto-plastic stress distribution model, which, however, requires numerous parameters that are challenging to obtain. Consequently, simplified linear elastic stress models have been widely adopted for their ease of parameterization. Kirsch [0] first proposed a linear elastic stress model applicable when the borehole is oriented towards the direction of the principal stress, while Fairhust [0] extended this to arbitrary borehole orientations. Sedimentary shales, treated as transversely isotropic materials, exhibit significant differences in elastic parameters between vertical and parallel bedding directions. However, studies suggest that elastic anisotropy has minimal impact on the safe density window of borehole walls compared to stress and strength anisotropy [10-0]. Current transversely isotropic elastic stress models only explain stress distribution at the borehole wall, prompting this study to utilize a homogeneous linear elastic stress model to investigate borehole integrity.

An important feature distinguishing shale from conventional reservoirs is its strength variability with bedding and load angles [0-15]. Jaeger [0], using the MC strength theory, proposed a weak plane strength theory that categorizes shale failure into intact and weak plane shear failure modes, effectively explaining shale strength anisotropy and widely applied in borehole stability analyses. Current methods involve direct shear experiments along bedding planes to obtain cohesion and internal friction angle of 60° bedding shales under different confining pressures [0-0]. However, these experiments only measure cohesion and friction angle within bedding planes and do not reflect the continuous influence of bedding angle variations on rock strength [0-0]. Moreover, shale's characteristics include

fine-layered structures, natural fractures, low permeability, and strong cation exchange capacity, making it sensitive to water-based muds and prone to severe borehole instability. Therefore, oil-based muds are extensively employed despite their higher costs and significant environmental hazards. The use of water-based drilling fluids in shale formations necessitates understanding their impact on shale structure and mechanics [0-0].

To elucidate shale borehole instability mechanisms under multi-field coupling environments, this study employs a multi-field coupled borehole stress model and integrates single weak plane rock strength criteria. A collapse pressure calculation model for shale boreholes is established, exploring the distribution patterns of borehole stress under multi-field coupling environments and obtaining collapse pressure contour maps for arbitrary borehole trajectories. The findings contribute to understanding shale borehole instability mechanisms and optimizing shale formation borehole trajectories.

2. Multi-field coupled wellbore stability model

2.1. Stress distribution model around wellbore

After drilling through geological formations, the stress concentration around the wellbore is influenced by the natural stresses in the surrounding rock. To convert these natural stresses into the wellbore's Cartesian coordinate system, it is essential to establish coordinate systems: the geodetic coordinate system (Xe-Ye-Ze), the stress coordinate system (Xs-Ys-Zs), and the wellbore Cartesian coordinate system (Xb-Yb-Zb). The transformation relationships between these coordinate systems are crucial. Figure 1 illustrates these coordinate systems where Xe-Ye-Ze represents the geodetic coordinate system, Xs-Ys-Zs represents the stress coordinate system, and Xb-Yb-Zb represents the wellbore Cartesian coordinate system. αs and βs denote the angles between the horizontal maximum stress direction and the true north direction, and between the horizontal maximum stress direction and the direction of the plumb bob, respectively. αb and βb represent the angles between the projection of the wellbore axis on the horizontal plane and the true north direction, and between the wellbore axis and the plumb bob direction, respectively. σH, σh, and σv represent the maximum horizontal stress, minimum horizontal stress, and vertical stress, respectively.

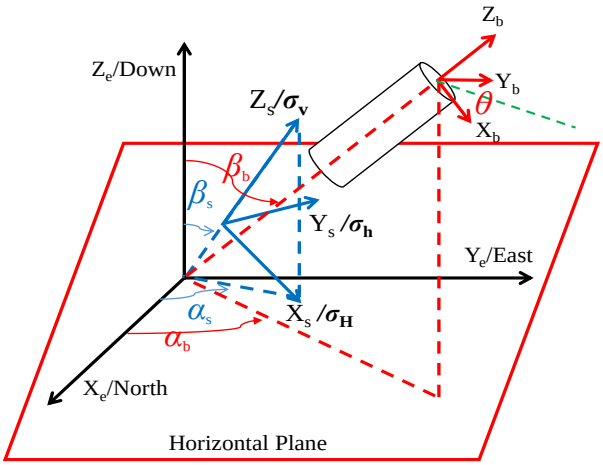

Figure 1. The transformation relationship between borehole column coordinate system stress and geodetic coordinate system, geo-stress coordinate system and borehole rectangular coordinate system

Based on the definitions provided, according to coordinate transformation theory, the natural stresses are first transformed into the geodetic coordinate system (Xe-Ye-Ze). Subsequently, these stresses in the geodetic coordinate system are further transformed into the wellbore Cartesian coordinate system (Xb-Yb-Zb). Ultimately, the stress components of the natural stresses in the wellbore Cartesian coordinate system can be expressed as shown in Equation 1,

$$\begin{cases} \sigma_{xx} = \sigma_H \cos^2\beta_b \cos^2(\alpha_b - \alpha_s) + \sigma_h \cos^2\beta_b \sin^2(\alpha_b - \alpha_s) + \sigma_v \sin^2\beta_b \\ \sigma_{yy} = \sigma_H \sin^2(\alpha_b - \alpha_s) + \sigma_h \cos^2(\alpha_b - \alpha_s) \\ \sigma_{zz} = \sigma_H \sin^2\beta_b \cos^2(\alpha_b - \alpha_s) + \sigma_h \sin^2\beta_b \sin^2(\alpha_b - \alpha_s) + \sigma_v \cos^2\beta_b \\ \tau_{xy} = -\sigma_H \cos\beta_b \cos(\alpha_b - \alpha_s)\sin(\alpha_b - \alpha_s) + \sigma_h \cos\beta_b \cos(\alpha_b - \alpha_s)\sin(\alpha_b - \alpha_s) \\ \tau_{yz} = -\sigma_H \sin\beta_b \cos(\alpha_b - \alpha_s)\sin(\alpha_b - \alpha_s) + \sigma_h \sin\beta_b \cos(\alpha_b - \alpha_s)\sin(\alpha_b - \alpha_s) \\ \tau_{xz} = \sigma_H \cos\beta_b \sin\beta_b \cdot \cos^2(\alpha_b - \alpha_s) + \sigma_h \cos\beta_b \sin\beta_b \sin^2\omega - \sigma_v \cos\beta_b \cdot \sin\beta_b \end{cases} \quad (1)$$

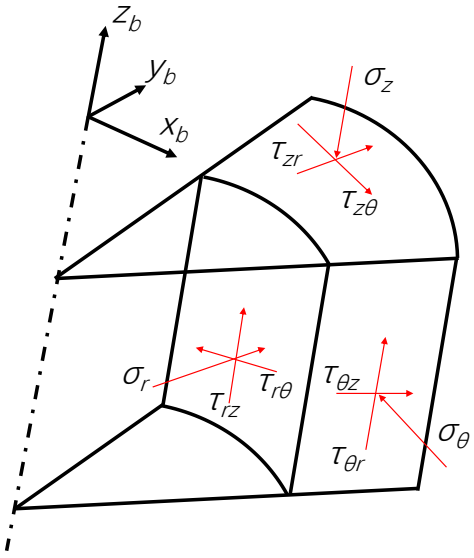

Figure 1. Stress State of Wellbore Rock Units

After drilling through the formation, the original stress state of the strata is disrupted, leading to a redistribution of stresses around the wellbore and causing stress concentration effects. Representing the stress distribution around the wellbore in polar coordinates is more convenient. Therefore, the stresses around the wellbore in the Cartesian coordinate system (Xb-Yb-Zb) are transformed into the polar coordinate system around the wellbore, as shown in Figure 2. This figure illustrates nine stress components of arbitrary rock units around the wellbore in the polar coordinate system. In the realm of elasticity, based on the principle of linear superposition and Biot's effective stress theory, the equation for the effective stress around an arbitrarily inclined wellbore can be expressed as Equation (2),

$$\begin{cases} \sigma_r = \dfrac{(\sigma_{xx}+\sigma_{yy})}{2}\left(1-\dfrac{r_w^2}{r^2}\right)+\dfrac{(\sigma_{xx}-\sigma_{yy})}{2}\left(1-4\dfrac{r_w^2}{r^2}+3\dfrac{r_w^4}{r^4}\right)\cos 2\theta+\tau_{xy}\left(1-4\dfrac{r_w^2}{r^2}+3\dfrac{r_w^4}{r^4}\right) \\ \qquad \sin 2\theta+P_w\dfrac{r_w^2}{r^2}-\alpha P_p \\ \sigma_\theta = \dfrac{(\sigma_{xx}+\sigma_{yy})}{2}\left(1+\dfrac{r_w^2}{r^2}\right)-\dfrac{(\sigma_{xx}-\sigma_{yy})}{2}\left(1+3\dfrac{r_w^4}{r^4}\right)\cos 2\theta+\tau_{xy}\left(1+3\dfrac{r_w^4}{r^4}\right) \\ \qquad \sin 2\theta-P_w\dfrac{r_w^2}{r^2}-\alpha P_p \\ \sigma_z=\sigma_{zz}-2\nu(\sigma_{xx}-\sigma_{yy})\dfrac{r_w^2}{r^2}\cos 2\theta-4\nu\tau_{xy}\dfrac{r_w^2}{r^2}\sin 2\theta-\alpha P_p \\ \tau_{r\theta}=\left[\dfrac{(\sigma_{xx}+\sigma_{yy})}{2}\sin 2\theta+\tau_{xy}\cos 2\theta\right]\left(1+2\dfrac{r_w^2}{r^2}-3\dfrac{r_w^4}{r^4}\right) \\ \tau_{rz}=\left[\tau_{yz}\sin\theta+\tau_{xz}\cos\theta\right]\left(1-\dfrac{r_w^2}{r^2}\right) \\ \tau_{\theta z}=\left[-\tau_{xz}\sin\theta+\tau_{yz}\cos\theta\right]\left(1+\dfrac{r_w^2}{r^2}\right) \end{cases} \quad (2)$$

In which, where r_W is the radius of the wellbore, in meters; r is the distance from any point around the wellbore to the wellbore axis, in meters; Pw is the bottom-hole fluid column pressure, in MPa; Pp is the formation pore pressure, in MPa; θ is the azimuth angle around the wellbore, which is the angle clockwise from a point around the wellbore to the Xb-axis, in radians; α is the Biot's effective stress coefficient, dimensionless and ranging between 0 and 1; $\left[\sigma_{xx},\sigma_{yy},\sigma_{zz},\tau_{xy},\tau_{yz},\tau_{xz}\right]$ represents the stress components of the original stress state of the formation in the wellbore Cartesian coordinate system before drilling, in MPa, as shown in Equation 1. Equation 2 considers the influence of stress on the distribution of stresses around the wellbore. However, after drilling through the formation, several additional factors come into play. Drilling fluid comes into contact with the surrounding rock, causing thermal exchange due to circulation—where the drilling fluid temperature is lower than that of the rock. Minerals within the rock can chemically react with the drilling fluid, leading to chemical stresses. Additionally, the difference in pressure between the original formation pressure and the pressure from the drilling fluid column results in fluid flow effects, creating seepage stresses. Research has shown that on the wellbore,

$$\sigma_T=\frac{\alpha_m E(T-T_o)}{1-\nu} \quad (3)$$

Where ν is the Poisson's ratio, E is Young's modulus, α_m is a volumetric thermal expansion coefficient of rock matrix (°K^{-1}), T is the circulation temperature (°K), and T_o is virgin rock temperature (°K).

Kadyrov (2012) describes the effects of flow-induced stresses in the equations that define the stress alteration at the wellbore when a radial flow is introduced due to the overbalanced or underbalanced drilling,

$$\begin{cases} \sigma_{r,f} = p_w - p_o \\ \sigma_{\theta,f} = -(1-\alpha)\dfrac{1-2v}{1-v}(p_w - p_o) \\ \sigma_{z,f} = -(1-\alpha)\dfrac{1-2v}{1-v}(p_w - p_o) \end{cases} \tag{4}$$

The calculation of the osmotic pressure can be helpful in determining the chemical interaction impact on the stress alteration at wellbore. The numerical equations for the osmotic pressure and its effect on the effective stresses acting at the borehole are formulated as follows,

$$\begin{cases} \sigma_{r,c} = 0 \\ \sigma_{\theta,c} = \alpha\dfrac{1-2v}{1-v}\Delta\prod \\ \sigma_{z,c} = \alpha\dfrac{1-2v}{1-v}\Delta\prod \end{cases} \tag{1}$$

In which,

$$\Delta\prod = I_m\frac{RT_o}{V_w}\ln\frac{\alpha_{w,df}}{\alpha_{w,sh}} \tag{2}$$

Where $\sigma_{r,c}, \sigma_{\theta,c}, \sigma_{z,c}$ are the alteration of radial, hoop and axial stresses due to the introduction of the osmotic pressure. α is the Biot's coefficient, and is Poisson's ratio, which are stress dependent values. *Im* is a reactivity coefficient which characterizes membrane efficiency, a dimensionless parameter and ranges from 0 to 1, R is the universal gas constant and equals 8.314 J/K.mole, *To* is the absolute temperature, K. *Vw* is the molar volume of the water (18.104m^3), *aw,df* and *aw,sh* are chemical activities of the drilling fluid and shale pore water, respectively. Chemical activity for fresh water equals to 1, and for salt water is less than 1.

Based on the superposition principle, a numerical model of the change of borehole wall stress is obtained, including the influence of chemical interaction, temperature change and flow-induced stress. The equation is as follows:

$$\begin{cases} \sigma_r = P_w - P_o \\ \sigma_\theta = \left(\sigma_{xx} + \sigma_{yy} - \left(P_w - P_o\right)\right) - 2\left(\sigma_{xx} - \sigma_{yy}\right)\cos 2\theta - 4\nu\tau_{xy}^b \sin 2\theta + \alpha\dfrac{1-2\nu}{1-\nu}\Delta\prod \\ \qquad + \dfrac{\alpha_m E\left(T - T_o\right)}{1-\nu} - \left(1-\alpha\right)\dfrac{1-2\nu}{1-\nu}\left(P_w - P_o\right) \\ \sigma_z = \sigma_{zz} - 2\nu\left(\sigma_{xx} - \sigma_{yy}\right)\cos 2\theta - 4\nu\tau_{xy}\sin 2\theta + \alpha\dfrac{1-2\nu}{1-\nu}\Delta\prod + \dfrac{\alpha_m E\left(T - T_o\right)}{1-\nu} \\ \qquad -\left(1-\alpha\right)\dfrac{1-2\nu}{1-\nu}\left(P_w - P_o\right) \\ \tau_{r\theta} = \tau_{rz} = 0 \\ \tau_{\theta z} = -2\tau_{xz}\sin\theta + 2\tau_{yz}\cos\theta \end{cases} \quad (3)$$

2.2 Jaeger's plane of weakness

Most sedimentary rocks, due to their unique diagenetic processes, exhibit anisotropic characteristics, with shale in particular showing pronounced anisotropy. Extensive research has been conducted on the anisotropic strength characteristics of shale, leading to the development of various predictive models. However, there is still no unified evaluation method established to date. Based on different classification criteria, existing anisotropic strength criteria can be categorized into different types: theoretical models and empirical relationship models based on whether they have theoretical foundations; shoulder-type, U-shaped, and oscillatory-type based on their envelope trends; and continuous-type and discontinuous-type based on their failure modes.

The failure modes of laminated shale can be classified into intact and weak plane shear failures. Therefore, many scholars believe that discontinuous-type criteria have clear physical meanings and can better explain the instability mechanisms of anisotropic rocks. Jaeger's weak plane criterion has been shown to conform to the anisotropic strength characteristics of shale rocks in most shale gas reservoirs worldwide. The physical concepts of cohesion and internal friction angle in this criterion are well-defined and widely applied in the petroleum industry. Therefore, this study adopts this criterion to fit experimental data. The discriminant for intact rock and bedding plane in Jaeger's weak plane criterion is shown below:

$$\sigma_1\text{-}\sigma_3 = 2\left(S_{\mathrm{o}} + \sigma_3\tan\phi_{\mathrm{o}}\right)\left(\sqrt{1+\tan^2\phi_{\mathrm{o}}} + \tan\phi_{\mathrm{o}}\right) \quad (4)$$

$$\sigma_1\text{-}\sigma_3 = = \frac{2\left(S_{\mathrm{bp}} + \sigma_3\tan\phi_{\mathrm{bp}}\right)}{\left(1 - \tan\text{-}\phi_{\mathrm{bp}}\tan\beta\right)\sin 2\beta} \quad (5)$$

In which, σ_1, σ_3 represent the maximum and minimum principal stresses, respectively, in MPa. $S_{\mathrm{o}}, S_{\mathrm{bp}}$ denotes the cohesion of the shale matrix and weak planes, also in MPa. $\phi_{\mathrm{o}}, \phi_{\mathrm{bp}}$ represents the internal friction angle of the shale matrix and weak planes, measured

in degrees. β represents the angle between the maximum principal stress and the normal to the weak plane, also in degrees, as illustrated in Figure 3.

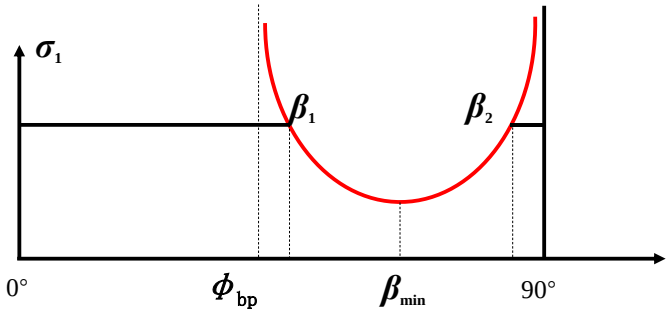

Fig.2 Jaeger' plane of weakness model failure envelops

Analysis of formulas 8 and 9 yields,

$$\begin{cases} \beta_1 = \phi_{bp}/2 + 0.5\arcsin\left\{\left[\left(S_{bp}\cot\phi_{bp} + \sigma_m\right)\sin\phi_{bp}\right]/\tau_m\right\} \\ \beta_2 = 90° + \phi_{bp}/2 - 0.5\arcsin\left\{\left[\left(S_{bp}\cot\phi_{bp} + \sigma_m\right)\sin\phi_{bp}\right]/\tau_m\right\} \end{cases} \quad (6)$$

Where σ_m, τ_m are respectively the maximum normal stress and maximum shear stress on the bedding plane in MPa. It can be seen that when β_1 approaches the internal friction angle of the bedding plane ϕ_{bp} or β_2 approaches 90 degrees, the rock strength predicted by equation 9 tends to infinity. As shown in Figure 1, according to formula 10, the bedding angle corresponding to the minimum strength can be obtained,

$$\beta_{min} = \left(\beta_1 + \beta_2\right)/2 = 45° + \phi_{bp}/2 \quad (7)$$

2.3 Wellbore collapse pressure calculation

Unlike the isotropic strength model, the anisotropic strength criteria of shale depend not only on strength parameters and confining pressure but also on the variable of bedding angle. In the analysis of borehole stability, it is necessary to determine the angle between the maximum principal stress and the bedding plane normal at each point around the wellbore. However, the determination of the direction of maximum principal stress around the wellbore is not straightforward. In the process of calculating wellbore collapse pressure, the minimum principal stress around the wellbore, equivalent to the hydrostatic pressure or radial stress, is crucial and more readily available in the Earth coordinate system. As shown in Figure 4, the angle between the minimum principal stress around the wellbore and the bedding plane normal can be obtained, where these two are complementary. Once the direction vectors of the bedding plane normal and the radial stress around the wellbore in the Earth coordinate system are obtained, the angle between them can be determined.

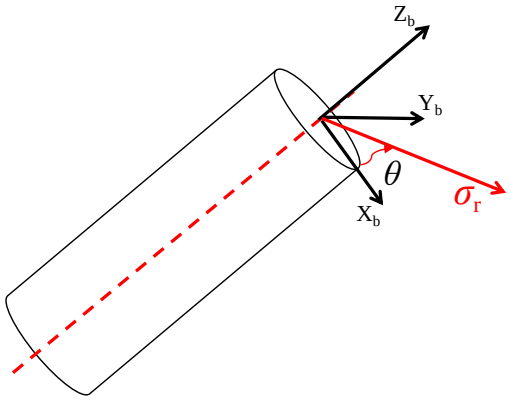

Figure 3. Reference coordinate systems of BPCS and GCS

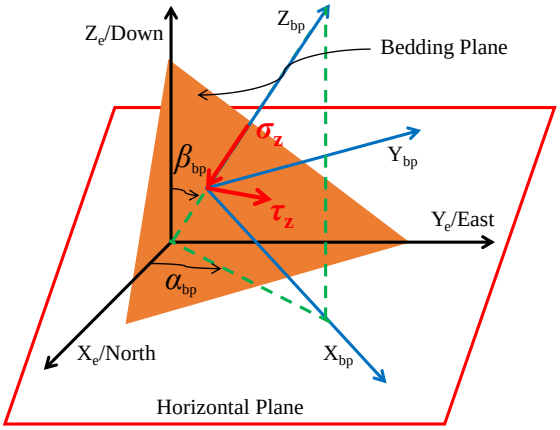

Figure 4. Reference coordinate systems of BPCS and GCS [1]

Figure 5 shows the orientation of bedding planes in the Earth coordinate system, α_{bp}, β_{bp} are the azimuth and dip of the bedding planes, respectively. The Z_{bp} axis represents the normal direction of the bedding plane. Therefore, in the Earth coordinate system, the normal vector of the bedding plane is expressed as Equation 12,

$$\mathbf{n}=[\cos\alpha_{bp}\sin\beta_{bp},\sin\alpha_{bp}\sin\beta_{bp},\cos\beta_{bp}] \quad (8)$$

As shown in Figure 5, the minimum principal stress at a point around the wellbore is the radial stress σ_r. In the wellbore Cartesian coordinate system Xb axis, rotated around Zb as the axis of rotation by a certain angle θ, represents the direction of the minimum principal stress. The coordinate transformation process from the Xb axis to the direction of σ_r is shown in Equation 13,

$$\mathbf{N}=\begin{bmatrix}\cos\theta & \sin\theta & 0\\ -\sin\theta & \cos\theta & 0\\ 0 & 0 & 1\end{bmatrix}\mathbf{X_b}=\begin{bmatrix}\cos\alpha_b\cos\beta_b\cos\theta+\sin\alpha_b\cos\beta_b\sin\theta\\ -\cos\alpha_b\cos\beta_b\sin\theta+\sin\alpha_b\cos\beta_b\cos\theta\\ -\sin\beta_b\end{bmatrix} \quad (9)$$

Here, the direction vector of the Xb axis is given by Equation 14,

$$\mathbf{X_b} = \left[\cos\alpha_b \cos\beta_b, \sin\alpha_b \cos\beta_b, -\sin\beta_b\right] \quad (10)$$

The sine of the angle between the normal vector of the bedding plane and the vector of the minimum principal stress around the wellbore gives the angle between the bedding plane normal and the direction of the maximum principal stress,

$$\beta = \arcsin \frac{\mathbf{n} \cdot \mathbf{N}}{|\mathbf{n}||\mathbf{N}|} \quad (11)$$

Since strength models typically use principal stresses, substituting the wellbore stress components into Equation 16 yields the principal stresses around the wellbore,

$$\begin{cases} \sigma_{1,2} = \left(\sigma_\theta + \sigma_z\right)/2 \pm \sqrt{\left(\sigma_\theta + \sigma_z\right)^2 + 4\tau_{\theta z}^2}/2 \\ \sigma_3 = \sigma_r \end{cases} \quad (12)$$

By incorporating Equations 15 and 16 into Jaeger's weak plane strength model, the stability status of each point around the wellbore can be assessed. Considering the periodicity and symmetry of azimuthal angles, subsequent analysis sets their range from 0° to 180° with a 2° increment. The range of wellbore inclinations is set from 0° to 90° with a 5° interval, and the azimuthal range of the wellbore is set from 0° to 360° with a 10° interval. A computational program is developed to calculate the collapse pressure at any point on the trajectory of the wellbore wall, with $r=r_w$ determined using Newton's iteration algorithm. For $r>r_w$, the stability of the surrounding rock at a distance r from the wellbore axis can be evaluated.

3.Results and analysis

3.1 Stress distribution around wellbore

Taking Well X in the shale oil block of the Qintong Depression in Northern Jiangsu Basin as an example, research was conducted to determine the reservoir's geomechanical parameters based on geological, drilling, and logging data of the well.

Table.1 Input parameters for a hypothetical case

Well depth /m	2538.4	Internal friction angle of weak plane /°	26
Vertical In-situ stress /MPa	48.64	Cohesion of weak plane /MPa	3.3
Horizontal minimum In-situ stress /MPa	42.36	Dip angle of weak plane /°	15.1
Horizontal maximum In-situ stress /MPa	45.13	Dip direction of weak plane /°	110.5
Pore pressure /MPa	25.87	Azimuth of maximum horizontal stress /°	N0°E
Elasticity modulus /GPa	15.77	Thermal expansion coefficient, C-1	$2.8*10^{-6}$
Poisson's ratio	0.34	Membrane efficiency, unitless	0.11
Internal friction angle of rock matrix /°	30.1	Chemical activity of shale pore water	0.81

Cohesion of rock matrix /MPa	7.3	Chemical activity of drilling fluids	0.72
Biot's coefficient, unitless	0.7	Formation temperature, °C	90.3

The summary of in-situ stress, pore pressure, and rock physical-mechanical parameters at a depth of 2538.4 meters in Well X is shown in Table 1. Based on the data in Table 1, input into the wellbore collapse pressure calculation model established in this paper, the effects of fracture surfaces, temperature, permeability, and chemical reactions on wellbore stability are studied. By incorporating the data from Table 1 into the model, the comparison between the effective stresses of the wellbore considering only stress and those considering multiple coupled effects such as temperature, permeability, and chemical reactions is depicted in Figure 6.

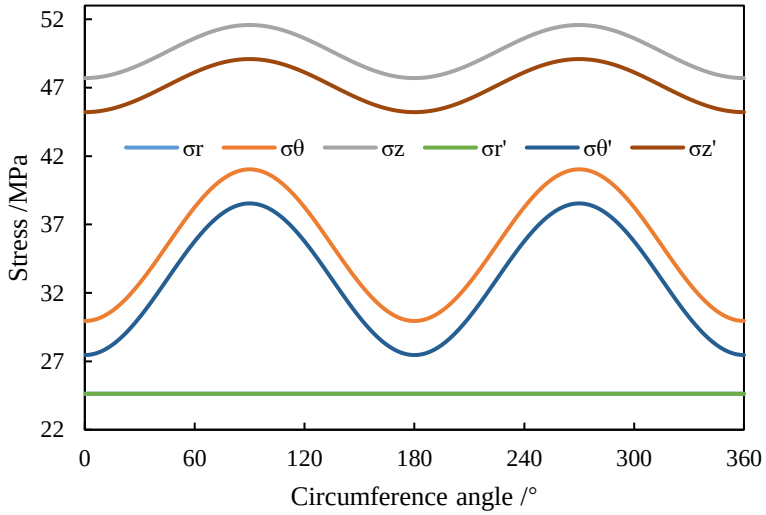

Fig.5 Effect of multi-field coupling on effective wall stress

In the figure 6, σr, σθ, and σz represent the radial, tangential, and axial effective stresses on the wellbore wall under stress conditions only. σr', σθ', and σz' represent the radial, tangential, and axial effective stresses on the wellbore wall under the coupled effects of multiple fields. From Figure 6, it can be observed that the radial effective stress remains constant with changes in azimuthal angle around the wellbore. The tangential and axial effective stresses vary sinusoidally with the azimuthal angle. After considering the effects of temperature, chemical reactions, and permeability, the tangential and axial effective stresses on the wellbore wall decrease, while the radial effective stress remains unchanged.

3.2 Wellbore collapse pressure

Based on the mineral composition and physicochemical characteristics of shale, shale typically exhibits certain hydration capabilities. The rock strength significantly decreases after interaction with drilling fluids. Additionally, shale formations often have well-developed bedding planes, where the structural and mechanical properties differ markedly from the rock matrix. These bedding planes can easily form high-permeability channels, facilitating the invasion of drilling fluids along them and further reducing the strength of the bedding planes, thereby increasing the risk of wellbore instability. Traditional wellbore stability analyses treat geological formations as isotropic materials, overlooking the influence of fractures on rock failure. To study the impact of fracture surfaces on wellbore stability, this study investigates the critical minimum drilling fluid density using Jaeger's Plane of Weakness criterion for preventing wellbore collapse in this block.

Using the data from Table 1 as input parameters and neglecting the effects of temperature, permeability, and chemical reactions, Figure 5 shows the contour map of the critical minimum drilling fluid density under stress considerations only. Figure 6 depicts the contour map of the critical minimum drilling fluid density required to maintain wellbore stability when considering the effects of temperature, permeability, chemical reactions, and stress. In these figures, colors ranging from deep blue to deep purple indicate increasing critical minimum drilling fluid density, while the radial direction represents the inclination angle of the wellbore, increasing outward from the center (representing vertical wells) to the boundary (representing horizontal wells). The angular direction represents the azimuthal angle of the wellbore, with 0° indicating the direction of maximum horizontal stress and 90° indicating the direction of minimum horizontal stress.

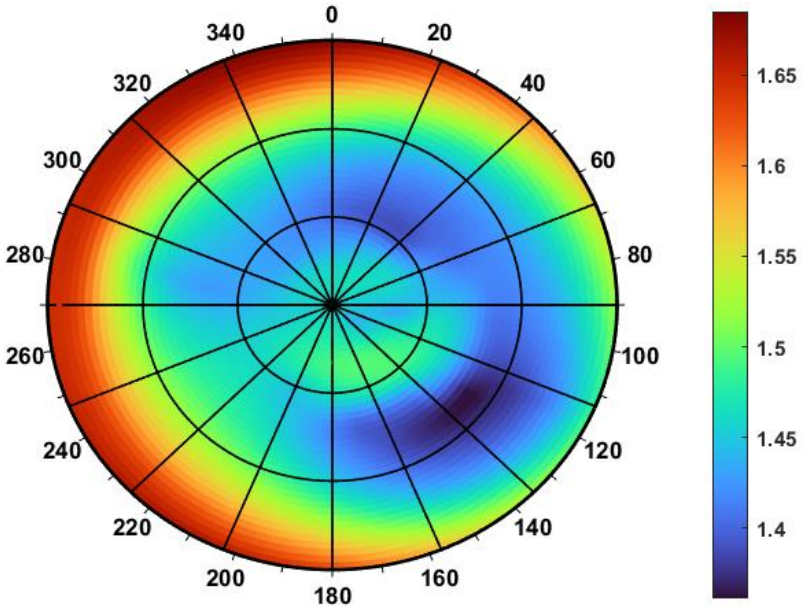

Figure 6. Cloud map of the lower limit of critical drilling fluid density to prevent wall collapse under stress only

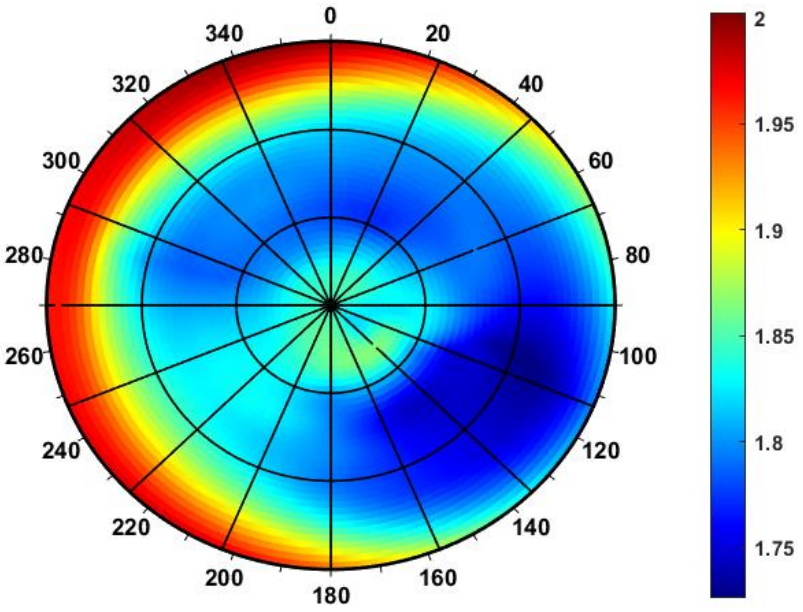

Figure 7. Cloud map of the lower limit of critical drilling fluid density to prevent wall collapse under multi-field coupling

From Figure 7, it can be observed that when considering only stress effects, the range of critical minimum drilling fluid density required to prevent wellbore collapse is between 1.3 and 1.7 g/mL. For horizontal wells with azimuth angles between 0° and 40°, and 180° to 360°, the highest critical minimum drilling fluid density increases from 1.4 g/mL to over 1.65 g/mL. For well trajectories around azimuth angles of 20° with inclinations near 30°, and azimuth angles of 140° with inclinations near 60°, the critical minimum drilling fluid density required to maintain wellbore stability is lower, below 1.4 g/mL, indicating better stability for wells drilled within this range. Considering the combined effects of temperature, chemical reactions, and permeability in a multi-field coupled environment, Figure 8 illustrates the contour map of the lower limit of the safe drilling fluid density window for wellbore stability. The critical minimum drilling fluid density ranges from 1.75 to 2 g/mL, and the contour map no longer shows a symmetrical distribution along the stress direction. For horizontal wells with azimuth angles between 0° and 40°, and 180° to 360°, the highest critical minimum drilling fluid density exceeds 2 g/mL. Wells with azimuth angles near 120° and inclinations near 60° exhibit the lowest critical minimum drilling fluid density, indicating better wellbore stability within this specific range of trajectories.

4.Conclusions

The study primarily concludes the following points,

(1) Under conditions considering only stress effects, the critical minimum drilling fluid density required to prevent wellbore collapse ranges from 1.3 to 1.7 g/mL. For horizontal wells with azimuth angles between 0° and 40°, and 180° to 360°, the highest critical minimum drilling fluid density increases from 1.4 g/mL to over 1.65 g/mL. This indicates that in these

azimuth and inclination combinations, a higher density drilling fluid is needed to maintain wellbore stability.

(2) Under the influence of multi-field coupling effects (including temperature, chemical reactions, and permeability), the range of critical minimum drilling fluid density extends from 1.75 to 2 g/mL. The contour map of critical minimum drilling fluid density no longer shows a symmetrical distribution along the stress direction, indicating that multi-field coupling significantly alters the stability of the wellbore and its demand for drilling fluid density. For horizontal wells with azimuth angles between 0° and 40°, and 180° to 360°, the lower limit of critical minimum drilling fluid density increases to above 2 g/mL, while in wells with azimuth angles near 120° and inclinations near 60°, the lower limit of critical minimum drilling fluid density is lowest, suggesting better stability in these regions.

(3) Through the study of drilling fluid density distribution under different conditions, it is found that the trajectory of the wellbore significantly influences wellbore stability. Particularly under certain azimuth and inclination combinations, adjustments in drilling fluid density are necessary to ensure wellbore stability. Therefore, in practical drilling operations, it is essential to comprehensively consider factors such as stress, temperature, chemical reactions, and permeability, optimizing drilling fluid density to enhance both wellbore stability and drilling efficiency.

References:

1. Abousleiman, Y., Tran, M., & Hoang, S. (2014). Mechanics of subsurface containment and hydraulic fracture containment: the important roles of coupled fluid flow and geopressure/stress state. Journal of Petroleum Technology, 66(11), 58-61.
2. Aadnøy, B. S., & Looyeh, R. (2011). Petroleum rock mechanics: drilling operations and well design. Gulf Professional Publishing.
3. Fjaer, E., Holt, R. M., Horsrud, P., Raaen, A. M., & Risnes, R. (2008). Petroleum related rock mechanics (2nd ed.). Elsevier Science.
4. Zhang, J. (2013). Borehole stability analysis accounting for anisotropies in drilling to weak bedding planes. International Journal of Rock Mechanics and Mining Sciences, 60, 160-170.
5. Maury, V., & De Gennaro, V. (1990). Integrated formation response using wireline log and drilling data: Application to drilling optimization. SPE Annual Technical Conference and Exhibition.
6. Plumb, R. A., & Edwards, S. (1992). Stress-induced borehole elongation: A comparison between the four-arm dipmeter and the borehole televiewer in the North Sea. SPE Formation Evaluation, 7(01), 13-18.
7. Tan, C. P., & Willson, S. M. (2012). The use of logging while drilling data in borehole stability analysis. Journal of Petroleum Science and Engineering, 88-89, 1-14.
8. Rahman, M. K., & Chilingarian, G. V. (1995). Drilling and drilling fluids. Elsevier.
9. Zhang, J., & Zhang, Y. (2017). Comprehensive wellbore stability analysis based on offset

well data and its application in deepwater drilling. Journal of Natural Gas Science and Engineering, 38, 494-504.

10. Yuan, Z., Zeng, Y., & Chen, M. (2014). Borehole stability of highly inclined wells in gas hydrate-bearing sediments. Journal of Petroleum Science and Engineering, 122, 224-232.
11. Ghassemi, A., & Zhang, Q. (2006). Poroelastic modeling of borehole stability in deformable fractured rock masses. Journal of Petroleum Science and Engineering, 52(1-4), 61-73.
12. Lee, D. S., & Haimson, B. (1993). Laboratory study of borehole breakouts in Lac du Bonnet granite: a case of extensile failure mechanism. International Journal of Rock Mechanics and Mining Sciences & Geomechanics Abstracts, 30(7), 1039-1045.
13. Chen, X., & Tan, C. P. (1993). A new approach to improve wellbore stability in shales. SPE/IADC Drilling Conference.
14. Dusseault, M. B., & Fordham, C. J. (1993). Time-dependent behavior of sands and sandstones. International Journal of Rock Mechanics and Mining Sciences & Geomechanics Abstracts, 30(2), 113-118.
15. Al-Ajmi, A. M., & Zimmerman, R. W. (2005). Stability analysis of vertical boreholes using the Mogi–Coulomb failure criterion. International Journal of Rock Mechanics and Mining Sciences, 42(3), 431-439.
16. Aadnøy, B. S. (1987). In-situ stress directions from borehole fracture traces. Journal of Petroleum Technology, 39(10), 1365-1370.
17. Fjaer, E. (2008). Reservoir geomechanics. Cambridge University Press.
18. Zhang, J., Lin, C., Tang, H., Wen, T., Tannant, D. D., & Zhang, B. (2024). Input-parameter optimization using a SVR based ensemble model to predict landslide displacements in a reservoir area–A comparative study. Applied Soft Computing, 150, 111107.
19. Lin, J., Dong, C., Lin, C., Duan, D., Ma, P., Zhao, Z., Liu, B., Zhang, X., Huang, X., 2024. The impact of tectonic inversion on diagenesis and reservoir quality of the Oligocene fluvial sandstones: The Upper Huagang Formation, Xihu Depression, East China Sea Shelf Basin. Marine and Petroleum Geology, 106860.
20. Wang Fengjiao, Xu He, Liu Yikun, et al. Mechanism of Low Chemical Agent Adsorption by High Pressure for Hydraulic Fracturing-Assisted Oil Displacement Technology: A Study of Molecular Dynamics Combined with Laboratory Experiments[J]. Langmuir, 2023, 39(46): 16628-16636.